

Theoretical and Experimental Studies of Micromachined Hot-Wire Anemometers

Fukang Jiang, Yu-Chong Tai
 EE 116-81, Caltech, Pasadena, CA 91125, USA
 Chih-Ming Ho, Rainer Karan, Michael Garstenauer
 MANE, UCLA, Los Angeles, CA 90024, USA

Abstract

A new type of micromachined and batch-fabricated hot-wire anemometers has been developed. The systematic characterization of these devices, especially of the steady-state characteristics, frequency response, and directional dependence are presented. These micromachined anemometers can perform better than conventional ones because of their extremely small size. It is demonstrated that a 10 μm long, 1 μm wide, and 0.5 μm thick polysilicon hot wire can have a unprecedented bandwidth of 1.4 MHz in constant-temperature mode.

1. Introduction

Hot-wire anemometers (as shown in Fig. 1a) have been used since the late 1800s. To date, they are typically made of platinum wires (usually 1mm long and 5 μm in diameter), and they are the most widely used devices for fluid mechanics measurements [1-4]. In general, it is favorable for the wire to have a small physical size for better performance. However, due to their small size the small size and mass production of them were not possible in the past because hand assembly was the only way to make them. Prototype micromachined anemometers have been explored [5,6], but they were never practical. It is therefore our intent to batch-fabricate high-performance hot-wire anemometers targeted for one-to-one replacement of the conventional ones.

Previously, we developed a new micromachining process to batch fabricate micron-size polysilicon wires intended for anemometer application [7]. It was encouraging that these micro-wires had unprecedentedly small time constants ($\sim\mu\text{s}$). Since then, we have implemented these hot wires into anemometers and performed calibration of them in wind-tunnels. Here, we report this study emphasizing the steady state response, the frequency response and the directional dependence of these anemometers operated in both constant current (CC) and constant temperature (CT) modes.

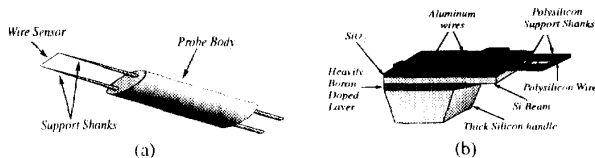


Fig. 1 Hot-wire anemometers: (a) Conventional, (b) Micro-machined.

2. Micromachined Hot-Wire Anemometers

The micromachined anemometers (Fig. 1b) consist of a sensing wire, two parallel support shanks, a silicon beam, and a thick (500 μm) Si handle [7]. The silicon beam is like the probe body and is 1 mm long, 200 μm wide and 75 μm thick. The two parallel support shanks are 100 μm long, 20 μm wide, and 0.5 μm thick. Various sizes of the sensing wires have been made and they are 10-160 μm long, 1 μm wide, and 0.5 μm thick. This structure is similar to the conventional anemometers so direct comparison can be made.

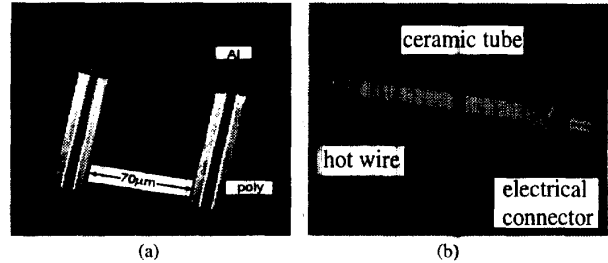


Fig. 2 (a) SEM of a micromachined hot wire (b) Micrograph of the anemometer packaging.

The package of the anemometers is a ceramic tube a few centimeter long and 3 mm in diameter. The anemometer handle is soldered with electrical cables, placed inside the tube, and then epoxy-fixed. During handling, all mechanical vibrations are avoided so as not to damage the wires.

3. Steady-State Characteristics

In steady state, the output characteristics of an anemometer should follow King's law [1-4] as,

$$IV = (K_0 + K_1 U^n) (T - T_a) \quad (1)$$

where I and V are the current and voltage drop across the wire, T is the average wire temperature, T_a is the ambient temperature, U is the flow velocity, K_0 and K_1 are the constants related to convective heat transfer. The exponent n depends on the hot wire geometry [8] and is about 0.5 for conventional hot wires. It can then be derived from Eq. (1) that in CC mode,

$$V_0 - V = \frac{AU^n}{1 + BU^n} \quad (2)$$

and in CT mode,

$$V^2 = A + BU^n \quad (3)$$

where A and B are velocity-independent constants.

The steady state characteristics of many hot wires with

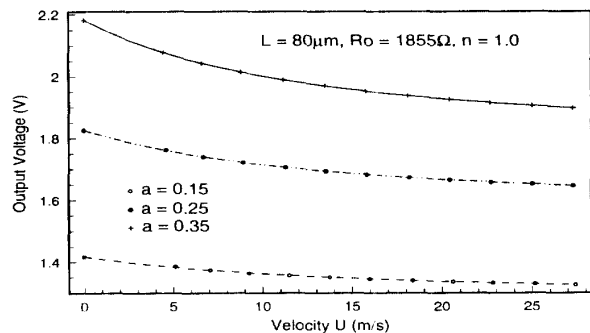


Fig. 3 Output characteristics of a 80 μm long hot-wire anemometer.

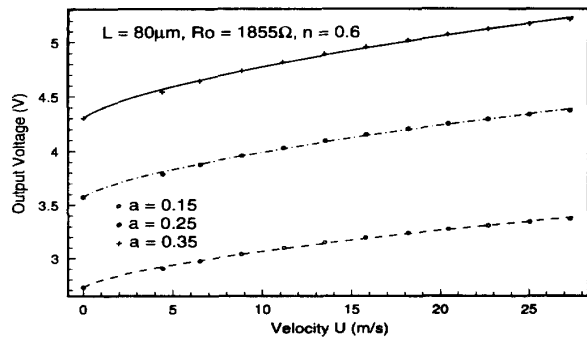


Fig. 4 Output characteristics of a 80 μm long hot-wire anemometer in CT mode.

lengths between 20-160 μm have been measured in wind-tunnels in both CC and CT modes. For example, Figs. 3 and 4 show the output characteristics of a 80 μm long hot-wire anemometer with different overhear ratios. The lines are the theoretical curves from Eqs. (2) and (3), and they agree well with the experimental results. However, it is interesting that for all the hot wires the value of n is close to 1 in CC mode and 0.6 in CT mode. The reason for the change of n from CC to CT mode is not known at the moment.

4. Frequency Response

In addition to steady-state response, dynamic response of an anemometer is also important especially for large Reynolds number flow measurements. In fact, the biggest advantage of the micromachined hot wires should be their improved bandwidth due to their extremely small sizes, i.e., low thermal masses.

4.1 Constant Current Mode

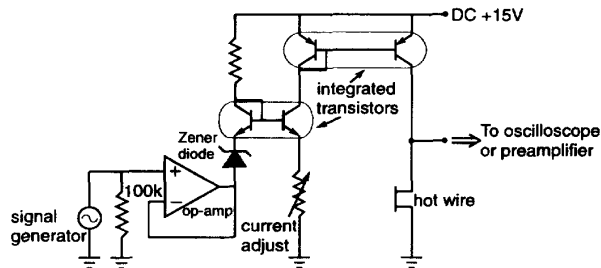


Fig. 5 The constant current anemometer circuit for time-constant and wind-tunnel testing.

Fig. 5 shows the circuit for the CC bias of a hot wire. To measure the time constant, we use either a square-wave or a sine-wave signal from the signal generator. The square wave is used if the hot wire has only one thermal time constant. This is often true for hot wires with aspect ratios larger than 200 [4]. For example, Fig. 6 shows a one-time-constant square-wave response of a hot wire with an aspect ratio of 300. On the other hand, if the aspect ratio of a wire is less than 200, its thermal response may have two time constants. One (τ_2) is associated with the sensing wire and the other (τ_1) with the wire support shanks. In this case, the square-wave method may not be accurate, and using sine wave signals to do the measurements in the frequency domain is suggested. Fig. 7 shows the measured total resistance of a 10 μm long wire as a function of frequency. Since the two time constants are different by more than an order of magnitude, this resistance can be accurately modeled by,

$$r = R + \frac{r_1}{1 + s\tau_1} + \frac{r_2}{1 + s\tau_2} \quad (4)$$

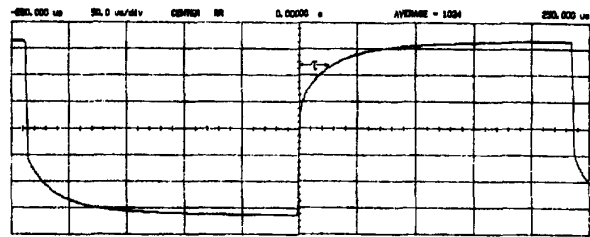


Fig. 6 Square wave response of a 200 μm long hot wire in C mode.

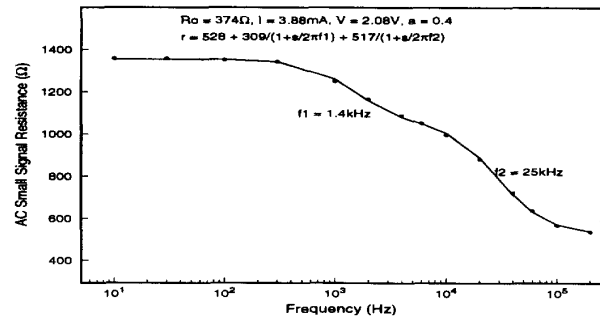


Fig. 7 Resistance change of a 10 μm long hot wire in frequency domain.

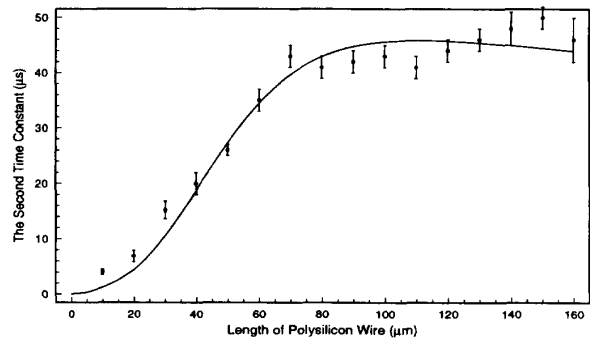


Fig. 8 Variation of the second time constant τ_2 with the wire length.

where R is the dc resistance, r_1 and r_2 are the amplitudes of the resistance change caused by ac heating effects. Fitting Eq. (4) into the experimental data in Fig. 7 then gives the two thermal time constants. For our hot wires, the ratio of r_2 to r_1 increases with the wire length l . The time constant associated with the support shanks, τ_1 , always ranges between 100 μs and 300 μs because of the fixed geometry design. The time constant with the wire, τ_2 , depends heavily on the length of the wire. In fact, it can be modeled [5],

$$\tau_2 = \tau_{21}\tau_{22}/(\tau_{21} + \tau_{22}) \quad (5)$$

$$\tau_{21} = \frac{\rho c_p}{(-\alpha J^2 \rho_0 + \frac{\kappa_{air} Nu}{wd})}, \quad \tau_{22} = \left(\frac{l}{\pi}\right) \frac{2\rho c_p}{\kappa_p}$$

where κ_{air} is the thermal conductivity of air; l , w , d are the length, width and thickness of the wire; ρ , c_p , ρ_0 , κ_p , α are the polysilicon's density, specific heat, resistivity at room temperature, thermal conductivity, and temperature coefficient of resistivity. It is clear that when l is small, the conduction time constant τ_{22} dominates and that τ_2 increases parabolically with l . If l is large, the convection time constant τ_{21} dominates and τ_2 becomes a constant. The measured τ_2 for our wires is shown in Fig. 8 with the theoretical fit from Eq. (5). As expected, the shortest wire (10 μm long) gives the smallest τ_2 of 4 μs . This corresponds to a bandwidth of 40 kHz, which is a significant

6.4.2

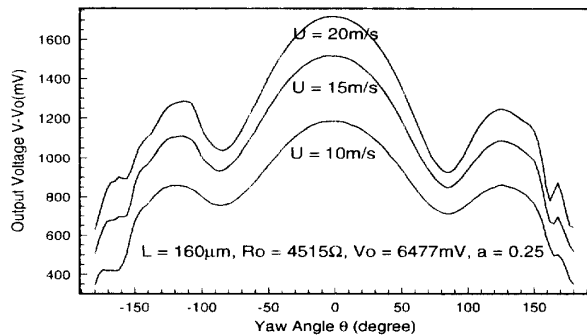


Fig. 13 Yaw angular dependence of a 160 μm long hot wire in CT mode.

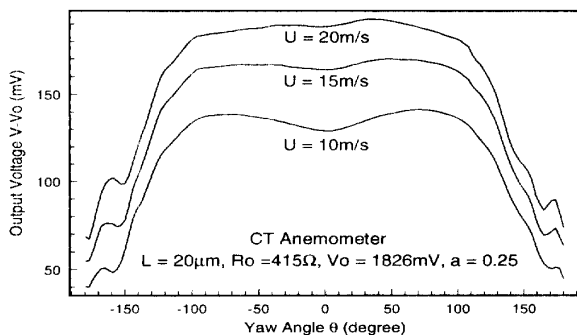


Fig. 14 Yaw angular dependence of a 20 μm long hot wire in CT mode.

third one is the varying effective cooling surface area during pitching. The first two effects tend to increase the cooling, while the third one depends on the wire geometry. For conventional hot wires, which are cylinders with large aspect ratios, only the first effect is present causing a 10 to 20 percent increase in output during pitching. However, for micromachined hot wires all three effects are significant because of the special structural design and the trapezoidal wire cross section (Fig. 12b). We expect strong pitch angular dependence for these hot wires, especially when l is small.

Figs. 15 and 16 are the measured pitch angular dependences of the same hot wires used in Figs. 13 and 14. The 20 μm long hot wire has much stronger pitch angle dependence than the 160 μm long one. This strong pitch angular dependence is useful for such a short wire because the yaw angular dependence is small. We noticed that the pitch characteristics are not symmetrical. One of the maxima occurs at $\phi = -90^\circ$ (when wind blows toward the bottom of the wire), while the other one occurs at $\phi = 60^\circ \sim 70^\circ$. We believe this is due to the trapezoidal wire cross section.

Finally, Fig. 17 shows the output characteristics of the same 20 μm long hot wire used above but at five different pitch angles in CT mode. The exponent n decreases from 0.58 to 0.50 as the pitch angle increases from 0° to 90° . We speculate that this is also because of the trapezoidal wire cross section.

6. Conclusion

A new type of micromachined hot-wire anemometers has been developed. Extensive characterization of the anemometers' steady-state characteristics, frequency response and directional dependence has been carried out. These anemometers, if properly designed, can be practical. They can significantly outperform conventional hot-wire anemometers, especially in terms of frequency response.

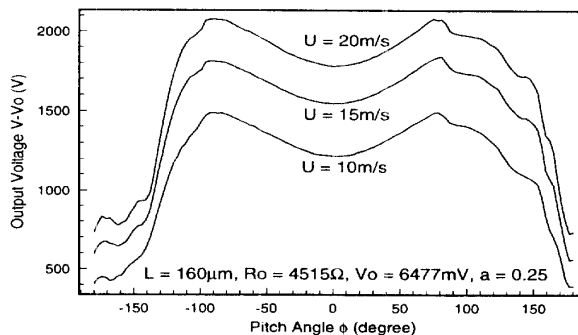


Fig. 15 Pitch angular dependence of the 160 μm long hot wire (also used in Fig. 13) in CT mode.

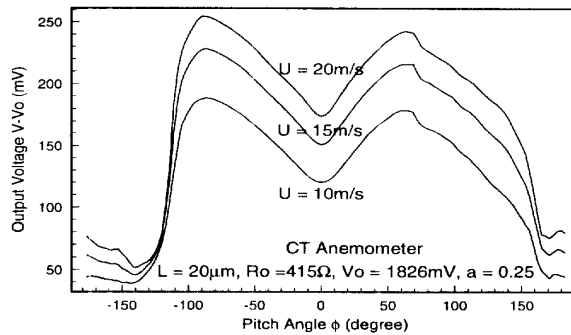


Fig. 16 Pitch angular dependence of a 20 μm long hot wire (also used in Fig. 14) in CT mode.

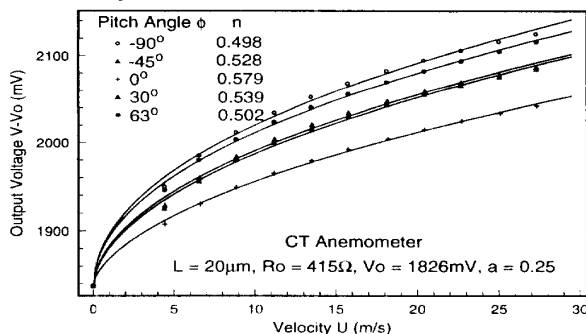


Fig. 17 Steady-state characteristics of a 20 μm long hot wire (also used in Figs. 14 and 16) in CT mode at different pitch angles.

Acknowledgments

This project is supported by AFOSR under grant F49620-92-J-0424. The authors would like to thank Trevor Roper for his help in processing.

References

- [1] A. E. Perry, *Hot-Wire Anemometry*, Clarendon Press, 1982.
- [2] C. G. Lomas, *Fundamentals of Hot Wire Anemometry*, Cambridge University Press, 1986.
- [3] R. F. Blackwelder, *Methods of Experimental Physics: Fluid Dynamics*, Vol. 18, Part A, Academic Press, 1981, pp. 259-314.
- [4] J. Goodstein, *Fluid Mechanics Measurements*, Hemisphere Publishing Corp., 1983, pp. 99-154.
- [5] Y. C. Tai, "Polysilicon Bridge for Anemometer Application", *Dig. Tech Papers, Transducers '85*, 1985, pp. 354-357.
- [6] L. Lofdahl, G. Stemme, B. Johansson, "Silicon Based Flow Sensors Used for Mean Velocity and Turbulent Measurements", *Experiments in Fluids*, Vol. 12, 1992, pp. 270-276.
- [7] F. Jiang, Y. C. Tai, C. H. Ho, W. J. Li, "A Micromachined Polysilicon Hot-Wire Anemometer", *Tech. Digest 1994 Solid-State Sensors & Actuator Workshop*, Hilton Head, USA, 1994, pp. 264-267.
- [8] M. Jakob, *Heat Transfer*, Vol. 1, John & Wiley, New York, 1949, pp. 559-564.

improvement over conventional hot wires (typical bandwidth of 700 Hz).

4.2 Constant Temperature Operation

Since the constant-temperature mode of hot wires uses negative feedback, it improves the frequency response significantly over the CC mode. Fig. 9 shows the circuit for our CT frequency response measurement. It is basically a Wheatstone bridge with a feedback operational amplifier. The ratio between R_2 and R_3 determines the gain, while R_1 is used to adjust the operating temperature of the hot wire. R_r and V_r are introduced here to adjust the quality factor Q in Eq. (6). The output voltage v_o of this circuit can be derived with the assumptions that the op-amp has a single pole at ω_0 and the hot wire has only one time constant, τ [3],

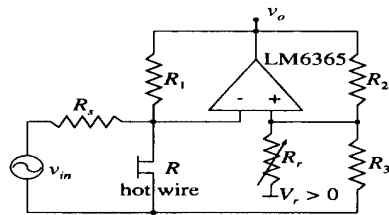
$$v_o = \frac{G_v \left(1 + \frac{s}{\omega_1}\right) v_{in} + S_u u}{1 + \frac{s}{Q\omega_2} + \left(\frac{s}{\omega_2}\right)^2} \quad (6)$$

and

$$\omega_1 = \frac{1}{(1+2a)\tau}, \quad \omega_2 = \sqrt{\frac{2aA_0\omega_0}{\tau} \frac{R_2 R_3}{(R_2 + R_3)^2}} \quad (7)$$

where G_v is the dc voltage gain, S_u is the dc velocity sensitivity, Q is the quality factor (always about 0.5 in our case), A_0 is the dc open loop gain of the op-amp, $a = (R - R_0)/R_0$ is the overheat ratio of the hot wire, and R_0 is the cold resistance. From Eq. (6), the CT anemometer is a second order system for both the electrical testing signal v_{in} and velocity signal u . Therefore, the electrical signal v_{in} is often used to calibrate the dynamic response of CT anemometers since sine or square wave velocity signals are difficult to obtain experimentally. It is worth noting that the gain-bandwidth product of the op-amp can limit the bandwidth of the overall circuit so to avoid this, a high speed op-amp should be used.

In the case that a hot wires has two time constants, the CT anemometer will behave like a third-order system. This will make the time-constant measurement difficult. Fortunately, our anemometers always have τ_2/τ_1 much larger than r_1/τ_1 (at least by an order of magnitude) so that Eqs. (6) and (7) can still be



$$R_1 \sim \frac{R_0^2}{R_3} (1+a) R_0, \quad R_r, R_3 \gg R_1, \quad R_2 \sim 8R_1$$

Fig. 9 The constant temperature anemometer.

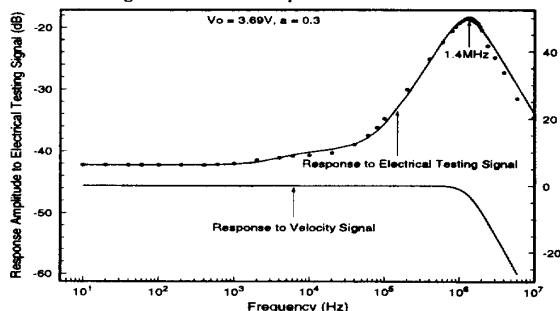


Fig. 10 Frequency response of a 10 μm long hot wire in CT mode.

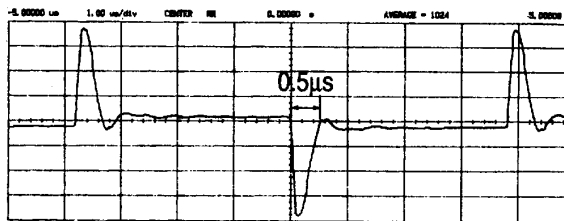


Fig. 11 Square wave response of the 10 μm long hot wire in CT mode.

used with little error. Fig. 10 then shows an example of the frequency response measured this way from a 10 μm long wire. In such a case, a very large bandwidth of 1.4 MHz is obtained. This is further verified by the square-wave response shown in Fig. 11, where the bandwidth is approximately $1/(1.3\tau_1) = 1.4$ MHz, with $\tau_1 = 0.5 \mu s$ as the peak width of the response curve [4]. Anemometers with bandwidths as high as 1.4 MHz have never been reported.

5. Directional Dependence

The directional dependence of the anemometer output voltage is important because it enables the determination of velocity vectors by using two or three hot wires oriented properly. For hot-wire anemometers, the output characteristics depend only on two angles: yaw angle and pitch angle. As defined in Fig. 12b, the yaw angle is the angle between the velocity vector U and its transverse component normal to the wire U_{\perp} , and the pitch angle ϕ is between U_{\perp} and the hot wire probe body axis y .

For large aspect-ratio hot wires, the transverse velocity component $U_{\perp} = U \cos \theta$ is mainly responsible for wire cooling by convection. A cosine-type response with respect to the yaw angle θ is then expected. This dependence is observed as shown in Fig. 13 for a 160 μm long hot wire in CT mode. The sharp voltage drop for the yaw angle higher than 90° is because the wire is in the wake of the probe body. In the extreme case such as a hot point sensor, there should be no directional dependence. Therefore we do not expect strong yaw angular dependence of the output for a small aspect-ratio hot wire. This is also confirmed in Fig. 14 for a 20 μm long hot wire. Interestingly, at low velocity, the output voltage increases with θ . This is because the longitudinal velocity component parallel to the wire U_{\parallel} contributes more to the wire cooling through the convection assisted heat conduction along the wire than U_{\perp} .

The pitch angular dependence of a hot wire can be attributed to three effects [2]. The first one is the hydrodynamic effect of the fluid passing through the opening bounded by the wire, support shanks, and the probe body when the pitch angle is increased. The second one is the additional cooling of the support shanks because they are oriented broadside to the flow during pitching. This effect is especially significant for shorter wires since more heat loss is through the support shanks. The

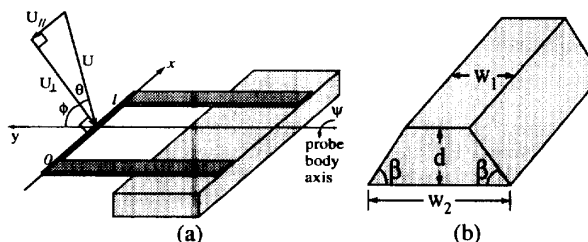


Fig. 12 (a) The yaw angle θ , pitch angles ϕ and roll angle ψ . (b) Cross section of micromachined hot wires.

6.4.4